Journal of Biomolecular NMR, 3 (1993) 215–224
ESCOM

J-Bio NMR 116

Efficient methods for obtaining phase-sensitive gradient-enhanced HMQC spectra

Alfred Ross, Michael Czisch, Christian Cieslar and Tad A. Holak*

Max-Planck-Institut für Biochemie, D-8033 Martinsried bei München, Germany

Received 4 December 1992
Accepted 2 February 1993

Keywords: Pulsed field gradients; HMQC; Proteins

SUMMARY

Three improved versions of the gradient-enhanced HMQC experiment are presented which yield phase-sensitive spectra with increased sensitivity compared to the recently described field-gradient HMQC schemes. The first method uses a complex linear back-prediction in order to generate the FIDs at the $t_1 = 0$. With this approach, refocusing pulses on the heteronucleus are not necessary. The sequence is especially useful for larger proteins with short relaxation times for the coherences that evolve during t_1. In the other two methods lower and shorter gradient pulses or asymmetric gradients are used to optimize sensitivity.

INTRODUCTION

A number of methods which allow for phase sensitive spectra in the gradient-enhanced spectroscopy have been proposed recently (Davis et al., 1991; Hurd et al., 1991; Boyd et al., 1992; John et al., 1992; Tolman et al., 1992; Vuister et al., 1992). In this communication, we introduce three improved versions of the gradient-enhanced (GE) HMQC experiment that, compared to the original field-gradient HMQC schemes, yield phase-sensitive spectra with increased sensitivity.

In general, a phase-sensitive 2D spectrum is obtained when contributions from two symmetrical coherence pathways of the opposite signs in the evolution dimension are combined in the final signal. In the HMQC experiment, there are four possible coherence transfer pathways that contribute the final signal (Bax et al., 1983; Ernst et al., 1987):

$$\begin{aligned}
&\text{(a) } I_z \rightarrow I_+ \rightarrow I_+S_+ \rightarrow I_-S_+ \rightarrow I_- \\
&\text{(b) } I_z \rightarrow I_+ \rightarrow I_+S_- \rightarrow I_-S_- \rightarrow I_- \\
&\text{(c) } I_z \rightarrow I_- \rightarrow I_-S_+ \rightarrow I_+S_+ \rightarrow I_+ \\
&\text{(d) } I_z \rightarrow I_- \rightarrow I_-S_- \rightarrow I_+S_- \rightarrow I_+
\end{aligned} \tag{1}$$

where I the proton spin and S is a heteronucleus spin.

*To whom correspondence should be addressed.

The 180-degree pulse at the proton frequency in the middle of the t_1 evolution period (Bax et al., 1983) causes inversion of the coherence order of the I-spin so that the pathways (a) and (c) precess with the effective frequency ω_s whereas (b) and (d) precess with $-\omega_s$. Signals resulting from the ω_s and $-\omega_s$ frequency pathways we call N-type and the latter P-type echoes, respectively, in analogy to the homonuclear N- and P-type echoes (Ernst et al., 1987).

Phase-sensitive gradient-enhanced spectroscopy has a reduced sensitivity when compared to a phase-cycled experiment because of supression of the N or P-type coherence pathways (Davis et al., 1992b). Sensitivity is reduced further because of the relaxation losses during gradient pulses, which are in the milliseconds range to completely dephase the unwanted signal contributions. These losses could be minimized by using stronger (and hence shorter) gradient pulses. However, very strong gradient pulses influence the stability of the spectrometer, producing eddy-currents which cannot be completely compensated for by adjustment of the pre-emphasis on the gradient unit. Delays have to be incorporated in the sequence that allow the eddy-currents to die away before the next pulse or acquisition. Our methods rely on shortening necessary delays and gradient pulses and therefore reducing relaxation losses.

METHODS

In the simplest gradient-enhanced HMQC experiment (Fig. 1A) (Hurd and John, 1991a), the minimum time for t_1 is given by the duration of the gradient pulses plus the time for the eddy-current relaxation. Besides relaxation losses of the double-quantum coherence, very large phase errors will be produced in the F_1-dimension that prevent or at least complicate phasing into the absorptive-mode line shapes. A possible approach for removing the phase errors in t_1 from gradient pulses is the use of a complex linear back-prediction, according to the Burg algorithm (Marple, 1987), in order to generate the FIDs that start at $t_1 = 0$ (Method A, Figs. 1A and 2A). When this approach is used, refocusing 180° pulses on the heteronucleus, as those present in the pulse sequence proposed by Davis et al. (1991), are not necessary. It is especially useful for proteins with short relaxation times of the coherences that evolve during t_1. The simplest gradient-enhanced HMQC sequence can be used, for example GE-HMQC (Hurd and John, 1991a) (Fig. 1B). Two FIDs per increment in t_1 are collected by inverting the first two gradient pulses from experiment to experiment (Fig. 1A), followed by the transformation to the States form as described below:

$$\begin{aligned} S_1(t_1,t_2) &= \cos(\omega_1 t_{1,\text{measured}}) \exp(-i\omega_2 t_2) \\ S_2(t_1,t_2) &= \sin(\omega_1, t_{1,\text{measured}}) \exp(-i\omega_2 t_2) \end{aligned} \tag{2}$$

Here, $t_{1,\text{measured}} = NE \times \Delta t_1 + 2 \times \tau_{\text{gradient}}$, NE number of increments in t_1, Δt_1 the evolution increment in t_1, and τ_{gradient} the duration of each gradient pulse. After a Fourier transform in t_2 on FIDs S_1 and S_2, a complex linear back-prediction is applied, in which the time domain signals for all $t_1 \leq 2 \times \tau_{\text{gradient}}$ at values $2 \times \tau_{\text{gradient}} - \Delta t_1$, $2 \times \tau_{\text{gradient}} - 2\Delta t_1$, $2 \times \tau_{\text{gradient}} - 3\Delta t_1$, ... are back-calculated. With these additional predicted data points, a Fourier transform in t_1 is done on the whole set and phasing of the resulting spectrum is possible.

The generation of the absorption-mode spectra from the P- and N-type FIDs is discussed below in more detail as there is some confusion in the literature, necessitating complicated processing schemes to be devised which do not allow for the final spectra to be phase-corrected in the F_2

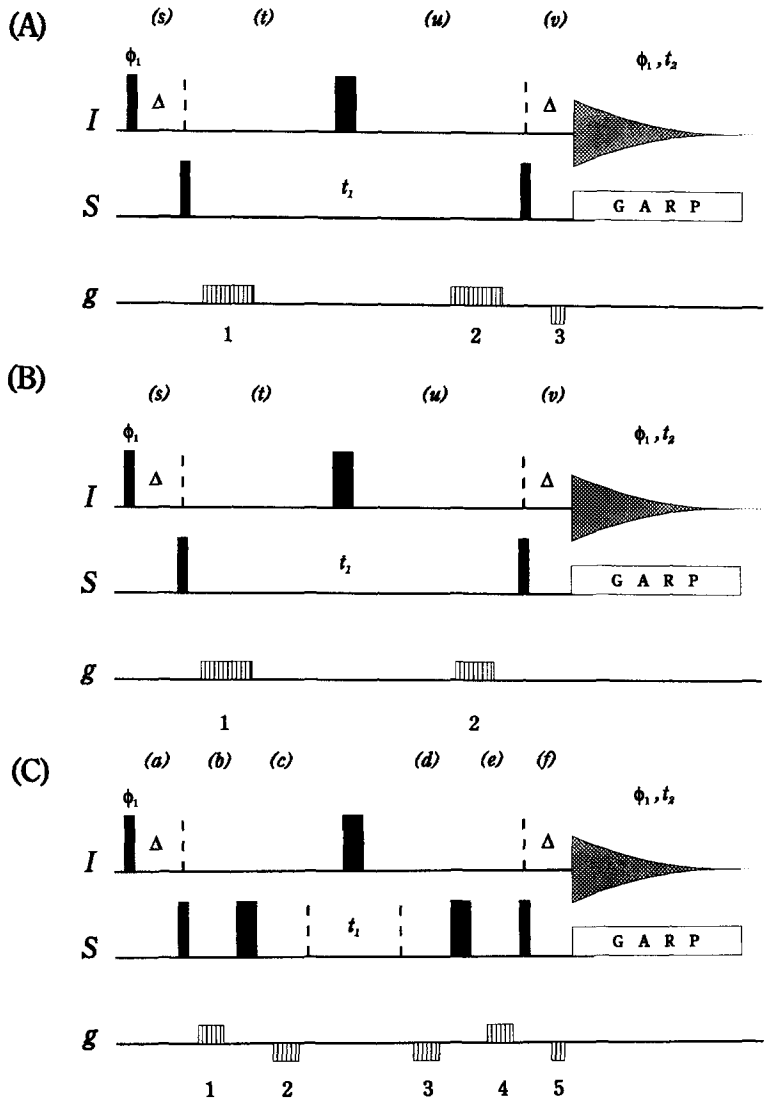

Fig. 1. Sequences of RF and gradient pulses used to record the HMQC spectra. Delay Δ was set to 4.8 ms for all pulse sequences. The GARP decoupling (Shaka et al., 1985) with a field strength of 1 KHz covering the whole measured ^{15}N sweep-width, was applied during acquisition. The strength of the 90° proton pulse was determined to be 20 KHz, the 90° nitrogen pulse was 14 KHz. The gradient strength was about 10 G/cm. The letters in parentheses above the pulse sequences indicate the position in the coherence level diagram of Fig. 2. Phase cycling (x,y−x,−y) was employed for the ϕ_1 and the receiver. No water suppression was employed. (A) A standard HMQC pulse sequence for gradient enhanced spectroscopy used together with the linear back-prediction method. The time which was back-predicted is equal the duration of the gradients (1) and (2) (each 2.47 ms) plus the delays used for relaxation of eddy-currents (each 100 μs). The t_1 increment was 200 μs; therefore 26 complex data points were back-predicted. To select necessary pathways for each increment two experiments with different sign of gradients 1 and 2 were employed. (B) Method B. Durations of the gradients were (1) = 2.47 ms, (2) = 2.02 ms. Coherence level selection was achieved by exchanging the two gradients. To have symmetry within t_1 with respect to the 180° pulse, a compensation delay of 450 μs (2.47–2.02 ms) was applied on the side of the shorter gradient. (C) Optimized refocused pulse sequence of Method C. For this sequence no linear back-prediction is necessary. Coherence level selection was achieved by switching the sign of the first four gradients.

dimension. For HMQC without field gradients, in which phase sensitivity with respect to t_1 is achieved by cycling the phase of the first 90° pulse on spin S according to the method by States et al. (1982), all pathways contribute to the detectable signal. The two signals detected for the two 90° shifts of the pulse ϕ are given by:

$$\begin{aligned} S(\phi = 0°) &= S_1(t_1,t_2) = \cos(\omega_1 t_1)\exp(-i\omega_2 t_2) \\ S(\phi = 90°) &= S_2(t_1,t_2) = \sin(\omega_1 t_1)\exp(-i\omega_2 t_2) \end{aligned} \tag{3}$$

The real parts of these complex signals S_1 and S_2 consist of the magnetization detected along the x-axis (stored at odd positions in an FID); the imaginary parts can be treated as the y-magnetization (stored at even positions in an FID). The signals are amplitude-modulated in t_1 and can be phased independently in F_1 and F_2. In contrast, if a de- and refocusing gradient sequence (Fig. 1) is applied and no phase shift of any pulse from increment to increment is performed only the pathways (a) and (d)(experiment 1) or (b) and (c)(experiment 2) of Eq. 1 survive the HMQC

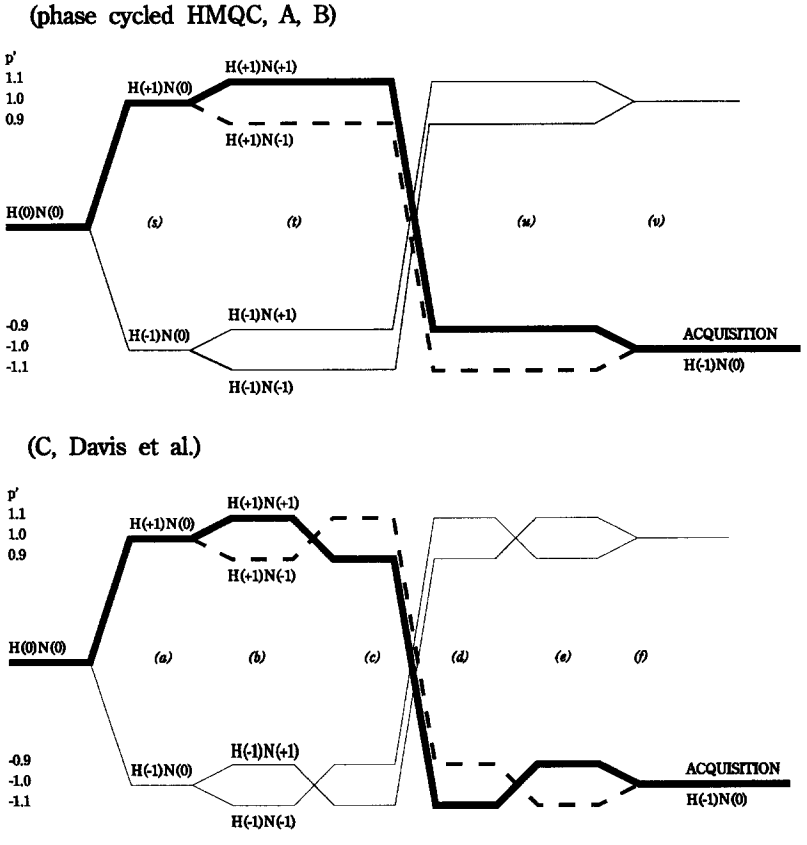

Fig. 2. Coherence level diagram for the experiments of Fig. 1. The top diagram describes experiments without 180° S-spin pulses (Methods A and B). The bottom diagram describes sequences with 180° refocusing pulses on the S-Spin. The numbers on the left side indicate the generalized coherence level if the S-spin is ^{15}N as $p' = (1 + \gamma_S/\gamma_I)$ (John et al., 1991). The letters in parentheses indicate the position within the pulse sequence of Fig. 1.

sequence. Neglecting relaxation during t_1 and t_2, these two pathways lead to the detectable signal:

$$\begin{aligned} &\text{(Experiment 1) } S_P(t_1,t_2) = \tfrac{1}{2} \exp(-i\omega_1 t_1)\exp(-i\omega_2 t_2) \\ &\text{(Experiment 2) } S_N(t_1,t_2) = \tfrac{1}{2} \exp(+i\omega_1 t_1)\exp(-i\omega_2 t_2) \end{aligned} \tag{4}$$

The real and imaginary parts (odd/even data points in the FID) of the signals S_P and S_N for each t_2 are now phase-modulated with respect to t_1, resulting in phase-twisted line shapes. Moreover, the discrimination of the sign of the precession frequency in t_1 cannot be determined for a single experiment. Contributions for which no double- and zero-quantum coherences are created, for example the water signal, remain defocussed during acquisition. However, the two data sets, corresponding to the P- and N-type spectra, recorded using the sequences in Fig. 1, can be processed to yield an absorption-mode spectrum in a procedure which can be illustrated in the following way.

We acquired for each increment t_1 an FID of the P-type and another FID for N-type echo. Each complex FID consists of R real (odd) and I imaginary (even) data points. Then for P-type echo signals for each t_1 increment we have:

$$S_P = [R_P(0),I_P(0)]\,[R_P(2dw),I_P(2dw)]\,[R_P(4dw), \ldots \tag{5}$$

and for N-type echo pathways,

$$S_N = [R_N(0),I_N(0)]\,[R_N(2dw),I_N(2dw)]\,[R_N(4dw), \ldots \tag{6}$$

where dw is the dwell time in t_2. New FIDs were calculated according to

$$S_1 = [R_P(0) + R_N(0),I_P(0) + I_N(0)]\,[R_P(2dw) + R_N(2dw),I_P(2dw) + I_N(2dw)] \ldots \tag{7}$$

and

$$S_2 = [I_P(0) - I_N(0),R_N(0) - R_P(0)]\,[I_P(2dw) - I_N(2dw),R_N(2dw) - R_P(2dw)] \ldots \tag{8}$$

These FIDs were processed to give the final phaseable spectra. The scheme is similar to a processing procedure for increasing the sensitivity of phase cycled HSQC spectra given by Palmer et al. (1991). In our case, no hypercomplex data are acquired and also the procedure of adding and subtracting the data is different. Our approach has the benefit that data manipulation can be easily performed on every spectrometer without the need of complicated data handling; only addition and subtraction are used within the serial FID files. Phasing in both dimensions can be performed after Fourier transforms in both dimensions. Another advantage of adding up two datasets with statistically independent noise is that the signal adds up to twice the intensity of a single experiment, whereas the noise becomes only $\sqrt{2}$ bigger (Wagner, 1989; Palmer et al., 1991). Thus, the signal-to-noise ratio for our phase-sensitive GE spectra is less than for spectra recorded with regular phase cycling by a factor of $\sqrt{2}$. This is better than gradient experiments that achieve

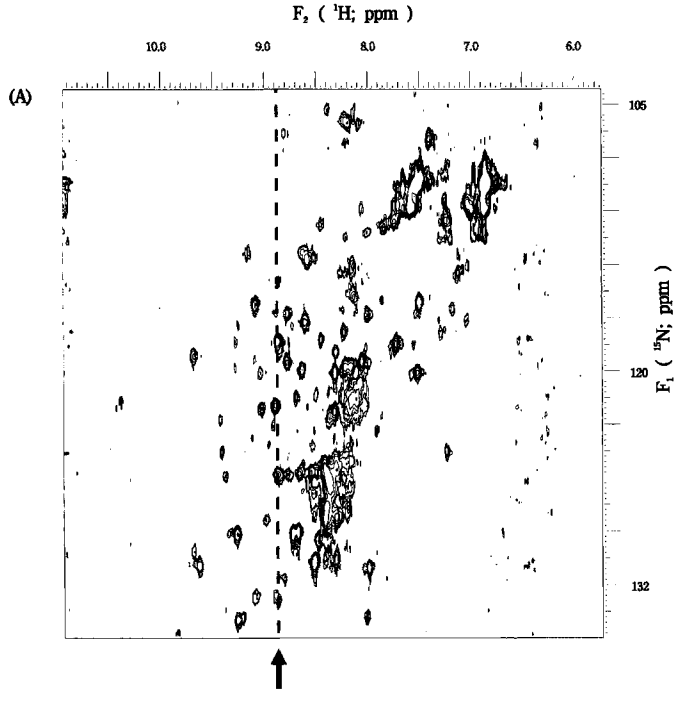

Fig. 3. Contour plots for the two HMQC spectra. (A) Phase-sensitive HMQC using TPPI in t_1 and phase cycling.

phase-sensitivity by collecting an FID that contains the N- and P-type echoes acquired in alternating scans; such gradient experiments are worse than regular phase cycling experiments by a factor 2.

Another method we introduce (Method B) is an asymmetric gradient experiment (Fig. 1B). Here, only two gradient pulses are applied during t_1, with no gradient before the acquisition. The selected pathways are given in Fig. 2B. Assuming that the strength of these two gradients is equal, their duration must satisfy the refocusing condition

$$(\gamma_I + \gamma_S)\tau_1 + (-\gamma_I + \gamma_S)\tau_2 = O$$
$$\frac{\gamma_I + \gamma_S}{\gamma_I - \gamma_S} = \frac{\tau_2}{\tau_1} \tag{9}$$

to proceed along the pathway indicated by a bold line in Fig. 2B. To retain the symmetry of t_1 with respect to the 180° pulse, an additional delay has to be added to the shorter gradient, compensating the difference of τ_1 and τ_2. For ^{15}N as the indirect observed nucleus, the ratio of the gradient duration is about 11/9. It must be inverted to 9/11 to obtain the pathway marked with a dashed line in Fig. 2B. Signals of protons not connected to nitrogen remain dephased with an absolute value of $\gamma_I(\tau_1 - \tau_2)$ in both cases. The longer pulse of 2.47 ms gave enough gradient strength to dephase all unwanted contributions. Again, the resulting data were processed as above, and a

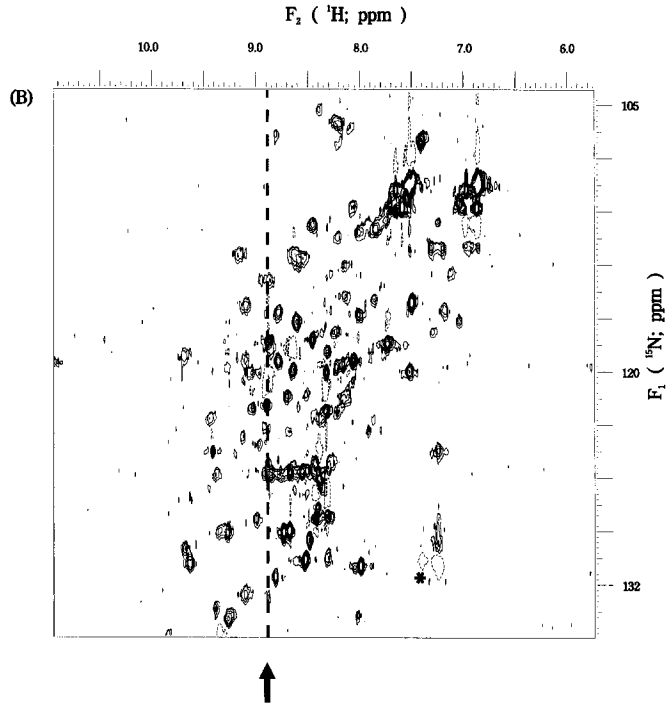

Fig. 3 (*continued*). Contour plots for the two HMQC spectra. (B) Spectrum recorded with Method A. The arrows indicate the position of the columns displayed in Fig. 4 for all experiments. The size of the data matrix was 256 × 2K data points in F_1 and F_2, respectively, covering 2000 Hz in F_2. In F_1 a $\pi/3$ shifted Q-sine window function, in F_2 a Gaussian window was applied in (B). One negative level was drawn with broken line to indicate artifacts from the linear back-prediction. Folded (negative) peaks are marked with asterisks.

complex linear back-prediction has to be applied to regenerate the final phasable spectrum. The benefit of this method lies in the fact that the last gradient pulse is shifted away from the acquisition. Thus, any contributions which might be refocussed due to field inhomogeneities before the data sampling is minimized. Also, eddy-currents are further reduced.

The last method we introduce (Method C) consists of a simple modification of the approach given by Davis et al. (1992b) for overcoming phase problems. In the original sequence, the precession of the spins during the two gradient periods is refocused by two 180° pulses. For each increment of t_1, two separated FIDs, one for the P-type and another for the N-type pathways, were acquired. Instead of using only two gradient pulses (number 1 and 4 in Fig. 1C), we applied two additional but inverted gradients (2 and 3) in the refocusing periods. A reduction of the length of the refocussing parts of the sequence by a factor of two is thus achieved. P- and N-type echo selection is accomplished by inverting either the last gradient (5) or the first four gradients (1–4) (Fig. 1C). We chose the latter version, because with the former a gradient echo of the water resonance was produced in one of the P- and N- experiments (the echo is caused by magnetic field inhomogeneities during acquisition). Directly before acquisition the net dephasing of the selected

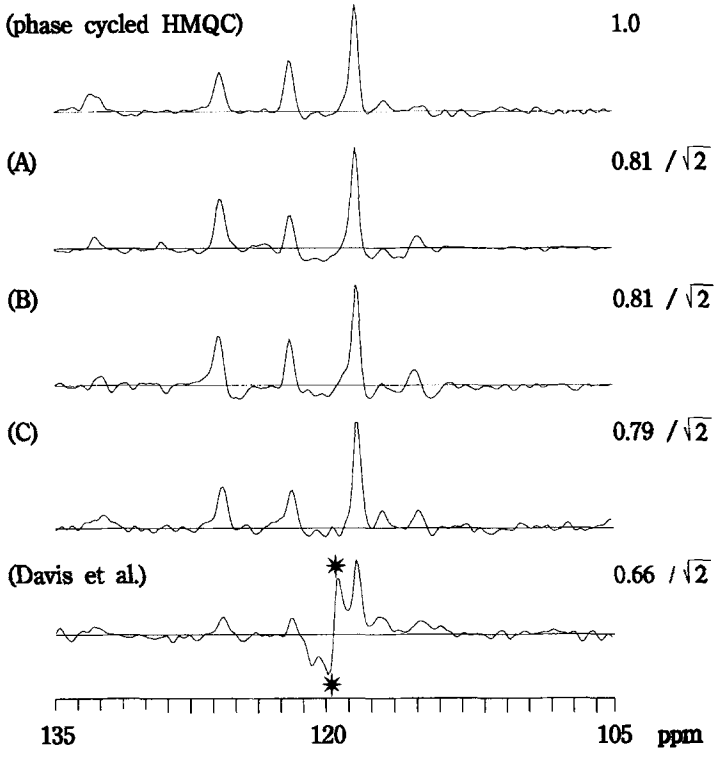

Fig. 4. The columns (indicated with an arrow in Fig. 3) taken from the 2D HMQC spectra. Displayed from top to the bottom are the columns from: the HMQC obtained with phase cycling and TPPI, (A) Method A, (B) Method B, (C) Method C and the HMQC acquired with the pulse sequence of Davis et al. (1992b) (an asterisk indicates the F_1 axial peaks). The numbers on the right-hand side indicate the calculated relative sensitivity referenced to the standard (phase cycled) HMQC (see text).

pathway has to be zero. In Fig. 2C, the two upper pathways during (b) and (c) lead to the detectable magnetization. Assuming the strength of all gradient pulses to be equal, the rephasing condition for these pathways is given by:

$$(\gamma_I + \gamma_S)\tau_1 - (\gamma_I - \gamma_S)\tau_1 - (\gamma_I - \gamma_S)\tau_1 + (-\gamma_I + \gamma_S)\tau_1 - \gamma_I\tau_2 = 0 \quad (10)$$

thus

$$4\gamma_S\tau_1 = \gamma_I\tau_2$$

where τ_1 and τ_2 are the durations of the gradient pulses in t_1 and before the acquisition, respectively, and γ_I and γ_S are the gyromagnetic ratios of the direct observed spin and the indirect observed spin, respectively. In the case of ^1H and ^{15}N, this ratio, γ_S/γ_I, is about 1:10. By inversion of the first four gradients, the pathway indicated by a dotted line in Fig. 2C would be selected.

EXPERIMENTAL

The pulse schemes A, B, and C were tested on a sample of ^{15}N-labeled, 3 mM solution of MPI

(mucous proteinase inhibitor, 107 amino acids) (Grütter et al., 1988) in 90% H_2O/ 10% D_2O. All experiments were carried out on a Bruker AMX-600 spectrometer equipped with a Bruker BGU gradient unit, limited only to rectangular shaped gradients along the z-direction and equipped with a 10 A amplifier and an actively shielded probehead. No presaturation was used in the gradient experiments. The maximum gradient strength was 10 G/cm, with gradient pulse durations between 500 μs and 2.47 ms. All 2D spectra were recorded with 256 experiments (i.e. for the gradient-enhanced spectra 128 increments for P-type and 128 increments for N-type echo pathways) and processed to 512 × 2K data points in F_1 and F_2 dimensions, respectively. The sweepwidth was 5000 Hz in F_1 and 4000 Hz in F_2. For the phase cycled HMQC, recorded for comparison, TPPI was used. Water was suppressed by presaturation in this experiment. For each gradient experiment, four scans were taken, with only CYCLOPS used on first proton pulse and the receiver. The total acquisition time for each complete gradient experiment was 56 min. If the complex linear back-prediction was applied, the first 26 t_1 increments were back-calculated using a prediction order of 35°. Back-prediction was carried out with our house-in written software CC-NMR on a CONVEX-C220.

DISCUSSION

Figure 3 shows the HMQC spectrum of MPI recorded with the aid of phase cycling and with Method A. Fig. 4 exhibits one of the columns for all the spectra taken for MPI. It can be seen from the Figs. 3 and 4 that the sensitivity is increased for all methods proposed in this paper in comparison to the spectrum taken with the pulse sequence of Davis et al. (1992b). In addition, in our spectra no F_1 axial peaks in the center of the spectra appeared. The main differences in the signal-to-noise ratio among the gradient experiments is due to the different starting points for $t_{1,measured}$ among the sequences. Failure to start the evolution at zero causes relaxation of the double-quantum coherence to diminish the amplitude of the signals. We estimated, from a qualitative examination of columns after the Fourier transform in t_2 only, that the relaxation time for double quantum coherence is T_{DQC} = 25 ms. In Fig. 4, at the right-hand side, numbers are given which were calculated for the GE experiments according to:

$$S/N_{GE} = S/N_{Phase,Cycl.}\ (1/\sqrt{2})\ \exp(-t_{1,start}/T_{DQC}) \tag{11}$$

where $t_{1,start}$ is the minimum t_1 equal to $2 \times \tau_{gradient}$. As described previously, the factor $\sqrt{2}$ has its origin in the addition of two datasets with statistically independent noise. This number indicates relative sensitivity for each experiment (assuming that $t_{1,start}$ for the experiment with phase cycling is equal 0). The result is in good qualitative agreement with the experimental spectra except that the refocused gradient experiment C gave spectra of lower quality than the those of Methods A and B. The difference can be explained by a larger number of pulses present in Method C which, due to their imperfection, reduce the signal-to-noise ratio. On the other hand, the sequence C is the easiest to carry out as it does not require the back-prediction treatment of the data. The best signal-to-noise ratio is exhibited by spectra obtained with Methods A and B. The amplitudes of some of the peaks in these spectra do not match the intensities in spectra recorded with phase cycling and those of Method C. The difference is caused predominantly by small errors in the first data points. In general, the application of the linear back-prediction may introduce incorrect

amplitudes and negative side-lobes at the very intense peaks (Fig. 3B). These artifacts, however, can be reduced when window functions and prediction order for the back-prediction is carefully optimized in the procedure.

The quality of water suppression by gradients depends strongly on the sign of the last gradient before the acquisition. The B_O field inhomogeneity during the acquisition partly refocuses improper selections, for example, the water signal. All gradient experiments were done with an receiver gain which was four times higher than the normal TPPI experiment, thus indicating good water suppression in the gradient experiments.

ACKNOWLEDGEMENTS

This work was supported by research grants from the Bundesministerium für Forschung und Technologie and from the Deutsche Forschungsgemeinschaft.

REFERENCES

Bax, A., Griffey, R.H. and Hawkins, B.L. (1983) *J. Magn. Reson.*, **55**, 301–307.
Boyd, J., Soffe, N., John, B., Plant, D. and Hurd, R. (1992) *J. Magn. Reson.*, **98**, 660–664.
Davis, A.L., Laue, E.D., Keeler, J., Moskau, D. and Lohman, J. (1991) *J. Magn. Reson.*, **94**, 637–644.
Davis, A.L., Boelens, R. and Kaptein, R. (1992a) *J. Biomol. NMR*, **2**, 395–400.
Davis, A.L., Keeler, J., Laue, E.D. and Moskau, D. (1992b) *J. Magn. Reson.*, **98**, 207–216.
Ernst, R.R., Bodenhausen, G. and Wokaun, A. (1987) *Principles of nuclear magnetic resonance in one and two dimensions*, Clarendon, Oxford, p. 316.
Grüttner, M.G., Fendrich, G., Huber, R. and Bode, W. (1988) *The EMBO Journal*, **7**, 345–351.
Hurd, R.E. and John, B.K. (1991) *J. Magn. Reson.*, **91**, 648–653.
Hurd, R.E., John, B.K. and Plant, H.D. (1991) *J. Magn. Reson.*, **93**, 666–670.
John, B.K., Plant, D., Heald, S.C. and Hurd, R.E. (1991) *J. Magn. Reson.*, **94**, 664–669.
John, B.K., Plant, D., Webb, P. and Hurd, R.E. (1992) *J. Magn. Reson.*, **98**, 200–206.
Marple, Jr., S.L. (1987) *Digital Spectral Analysis* Prentice Hall Inc. Englewood Cliffs, New Jersey, p. 240.
Shaka, A.J., Baker, P.B. and Freeman, R. (1985) *J. Magn. Reson.*, **64**, 547–551.
Palmer III, A.G., Cavanagh, J., Wright, P.E. and Rance, M. (1991) *J. Magn. Reson.*, **93**, 151–170.
States, D.J., Haberkorn, R.A. and Ruben, P.J. (1982) *J. Magn. Reson.*, **48**, 268–292.
Tolman, J.R., Chung, J. and Prestegard, J.H. (1992) *J. Magn. Reson.*, **98**, 452–467.
Vuister, G.W., Ruiz-Cabello, J. and van Zijl, C.M. (1992) *J. Magn. Reson.*, **100**, 215–220.
Wagner, G. (1989) *Methods in Enzymology*, **176**, 93–114.